Experimental investigations and variability considerations on 3D interlock textile composites used in low velocity soft impact loading

Frédéric Dau, M.-L. Dano, Yann Duplessis Kergomard

Experimental investigations and variability considerations on 3D interlock textile composites used in low velocity soft impact loading

F. Dau [a,*], M.-L. Dano [b], Y. Duplessis-Kergomard [a]

[a] Institut de Mécanique et Ingénierie de Bordeaux (I2M), Département DUrabilité Matériaux Assemblages Structures (DUMAS), Arts et Métiers ParisTech, esplanade des arts et métiers, 33405 Talence, France
[b] Université Laval, département de génie mécanique, Québec, Québec G1V0A6, Canada

A B S T R A C T

This study investigates the performance of three-dimensional (3-D) woven interlock composite plates subjected to impact loading. Low velocity (lower than 10 $m \cdot s^{-1}$) impacts with highly deformable rubber impactor are addressed. Response variability is investigated by conducting several impact tests in the same conditions. The effect of mass and velocity on damage tolerance is studied by varying the impact conditions. Force–time, displacement–time and force–displacement curves are first analyzed in such various impact conditions. Secondly, damage mechanisms are highlighted through microscopic observations. The large geometrical deformation of the rubber impactor during impact leads to a loading less localized than for a hard impactor which induces a wide spread damage distribution. Comments on the relations between damage states and mass–velocity conditions are proposed.

Keywords:
Variability
Damage
Textile composite
Soft impact
Micrographic study

1. Introduction

Composite materials are increasingly being used for primary aircraft components because of their superior structural performance such as high strength, high stiffness, long fatigue life, and light weight. These structures are prone to impact loading during their service life. Impact on composite structures has been largely studied [1–4].

Conventional laminated composite have fibers only oriented in the plane of the laminate and are therefore vulnerable to delamination during impact. Three-dimensional (3-D) woven composites offer a better delamination resistance and damage tolerance because of through-the-thickness yarns. Therefore, interest for using 3-D woven composites for aircraft applications is growing. Several studies have already shown that 3-D woven composites have superior impact performance than 2-D laminates [5].

The current study focuses on a special kind of 3-D woven composite called 3-D interlock woven composite. Some authors have already studied interlock composites behavior under high velocity ballistic impact [6]. However, impact can be of many different types. Impact can be caused for example by a bird or a runaway debris strike, a tool drop or by hail. Therefore, impact can be of low or high velocity and the impactor hard, soft or fragmentable. The impacted structure will behave differently dependently of the impact nature. Some investigations referenced in literature on the behavior of 3D woven composite subjected to rigid impact showed both increases and decreases in strength compared to an equivalent 2D woven laminates [7–10].

In this work, the behavior of a 3-D interlock woven composite under low velocity impacts (lower than 10 $m \cdot s^{-1}$) with highly deformable rubber impactors, also called soft impactors, will be studied. Such characteristics may correspond to a tire debris impact on an aircraft composite part for instance; it is complementary to high velocity impact of soft body such as birds [11,12]. This work follows on an investigation performed within a national research project on vulnerability of composite structures, which partly addressed the impact performance of different 3-D interlock carbon woven composites. The investigation which was both experimental and numerical [13–15] showed that the major damage mechanisms were yarn decohesion, matrix cracks and a few yarn ruptures mainly located at the back side of the composite plate. Three different reinforcement types with different ratios of 3D warp yarns to straight warp yarns (30%, 55% and 100%) were tested [14]. Results showed that for the same impact energy, damage decreases with an increasing ratio of 3D warp yarns. Thus, the higher the ratio of 3D warp yarns to straight warp yarns is, the higher the impact resistance is. However, a reinforcement with a high amount of undulated yarns has reduced in-plane properties [14]. Therefore, the reinforcement with 55% 3D warp yarns seems to offer a good compromise between impact damage tolerance and good stiffness properties.

* Corresponding author.
E-mail address: f.dau@i2m.u-bordeaux1.fr (F. Dau).

http://dx.doi.org/10.1016/j.compstruct.2016.06.034

This work will focus on the impact behavior of composite plates made with 3-D interlock carbon woven reinforcement using 55% 3D warp yarns. Variability issues will be investigated by performing repeated impact tests in the same conditions and the mass velocity effect on damage tolerance will be studied by varying the impact conditions. First, the materials used for the impactor and the composite plate are described. Then, the experimental set-up is explained. Next, the variability study is presented and the results are analyzed. Finally, the experimental results obtained for the mass velocity effect study are discussed. Force–time, displacement–time and force–displacement curves and damage mechanisms observed on micrographies are particularly commented.

2. Materials

2.1. Rubber impactor

The impactor is made from Styrene–Butadiene–Styrene (SBS) rubber which is a hard and durable rubber material typically used for aircraft tires or shoe soles. A SBS rubber impactor with a shore A hardness (SHA) [16] of SHA-60 was selected and especially manufactured for this study. As shown in Fig. 1, the impactor was selected to have a simple regular and hemispherical shape in order to reduce the complexity of this study. The diameter of the impactor is $\Phi = 70$ mm. The hemispherical piece of rubber was bonded during the process to a steel cylinder. A steel screw part allows fixing of an additional part that includes the force sensor. Finally, the impactor instrumented with the force sensor is fixed on a carriage to constitute the full mass.

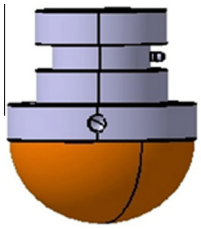

Fig. 1. Hemispheric rubber impactor.

It is known that the Mullins effect [17] may induce a change in the behavior of newly manufactured rubber during the first tests. To prevent this effect from occurring, ten quasi-static compression cycles with a maximum load of 20 kN were performed on the rubber impactor. Moreover, the control of the rubber chemical composition during the manufacturing leads to a behavior much more elastic than viscous. Then, the strain rate effects were reasonably neglected.

2.2. Interlock 3X woven composite target

Impact tests were performed on an interlock 3X woven composite plate. The fabric was composed of warp weaver (or 3D warp) yarns, stuffer (or straight warp) yarns and filler (or weft) yarns as depicted in Fig. 2a. The ratio of 3D (deviated) warp yarns to straight warp yarns was equal to 55%. The present fabric can be defined as a 3D warp interlock A-T 9-5 {5-4} according to the general definition of 3D warp interlock fabric referenced in [18]. Both the warp and the weft yarns were manufactured with carbon HR Tenax-E HTS40 F13 12K 10Z yarns. The areal density of interlock 3X is 2720 g/m^2. A three-dimensional micro-computer-tomography (micro-CT) scan of the dry 3X 55% material is shown in Fig. 2b.

The interlock 3X woven fabric was processed by Resin Transfer Molding (RTM) using a RTM6 epoxy resin. The resin was injected at 120 °C and the composite plate was cured at 160 °C. The thickness of the interlock fabrics dryness is 10 mm thickness before injection whereas the final thickness of the plates is 2.7 mm. The useful dimensions of the plates issued from the RTM process are 500 mm × 500 mm. Micrographs on Fig. 3 illustrate the cross

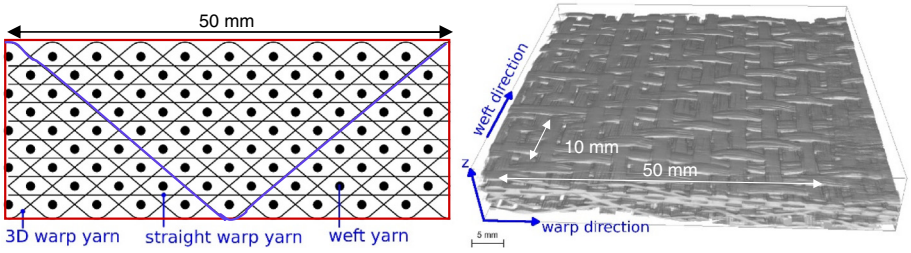

(a) Diagram of the cross section unit cell (b) Micro-CT scan

Fig. 2. 3D interlock 3X 55% woven composite.

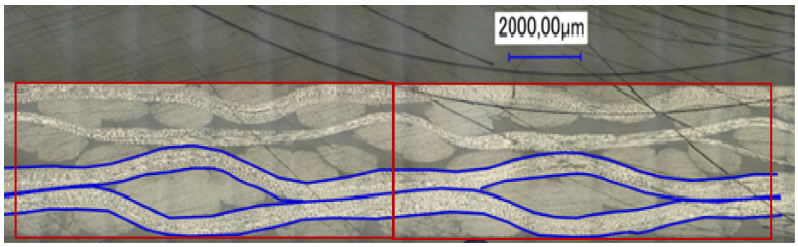

(a) Along the weft direction

(b) Along the warp direction

Fig. 3. Micrographs of the 3D interlock 3X 55% woven composite cross section.

section of the composite along the weft and the warp directions. The representative unit cell is represented by the rectangle. One can estimate that the unit cell has a thickness of 2.7 mm, a length L_{warp} of about 50 mm in the warp direction, and a width L_{weft} of about 10 mm in the weft direction. The dimensions are also indicated in Fig. 2.

During manufacturing, the fabric is not stretched and is compacted from 10 mm to 2.7 mm by closing the mold. The yarns are then rearranged in such a way that the weft yarns do not remain straight but wave significantly in a repetitive manner as depicted in Fig. 3a. The through-thickness warp yarns as for them seem to wave moderately along their woven pattern, Fig. 3b.

Fig. 4 shows a close-up of the interlaced weft and warp yarns. One can see that the fiber volume fraction within a yarn is uneven probably caused by compaction during the RTM process. Some resin rich areas are clearly visible and can take the form of paths within the yarn. On the contrary, the resin cannot impregnate very well the areas where the yarns are brought into contact during compaction. Therefore, the rearrangement of the yarns by compaction and their impregnation during the RTM process introduce a natural variability.

3. Experimental set-up

The impact tests were performed on the home made drop tower illustrated in Fig. 5a. The composite specimen was simply supported along a circular perimeter of diameter Φ_{BC} = 154 mm as shown in Fig. 5b. The ratio $\Phi_{BC}/\Phi_{impactor}$ = 2.2 was adopted to avoid boundary effects.

The composite specimens were square with a side length equal to 180 mm. On the top surface, a piece of paper was taped to obtain a print of the impactor during testing. On the other side a speckle pattern was sprayed to allow measurement of the displacements and strains using a digital image correlation (DIC) system. The plate was then placed on the bottom support and the top part was assembled with four bolts tightened with a torque of 80 mN.

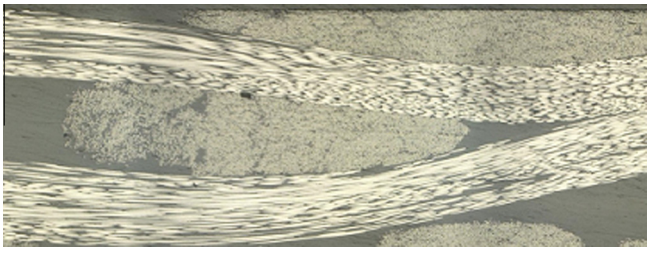

Fig. 4. Details of the interlock 3X 55% woven composite microstructure.

The contact force history between the elastomer and the composite specimen was measured by a piezoelectric sensor.

The impactor was covered with blue chalk before each test. Therefore the maximum contact area could be determined from the print of the impactor on the paper taped on the target. The displacement history of the carriage was measured by a laser sensor so that the velocity of the falling mass can easily be assessed. Moreover, one high speed camera was used to record images of the back of the specimen during impact. The acquisition speed was 8400 image/s to get a good resolution. Due to a lack of available space between the specimen and the ground, a set of two mirrors assembled with hinges inclined at a 45° angle relative to the ground was placed under the composite plate. The two mirrors provided two images of the backside of the specimen that could be recorded by only one camera.

After impact, microscopic observations were done on interlock samples cut from the tested plates in order to analyze induced damage.

4. Experimental test program

A series of experimental tests were carried out using five incident energies: 202 J, 238 J, 272 J, 307 J and 346 J. These theoretical energies were imposed by the impactor mass/incident velocity couple. Three masses were selected for the test campaign: 9.9 kg, 13.9 kg and 17.9 kg. The incident velocity was then enforced by the drop height. For some energy levels, tests were conducted several times. Table 1 summarizes all the tests that were carried out.

After testing, microscopic observations were done on material samples cut from plates that were tested at 202 J, 238 J and 272 J energy levels as indicated in Table 1. The samples were cut along the weft and warp directions at the center of the plates as depicted in Fig. 6. Referring to the figure, specimen noted S_{wa} allows observ-

Table 1
Tests matrix.

Test	Energy (J)	Mass (kg)	Speed (m/s)	Height (m)	Micrography
1	202	9.9	6.38	2.08	x
2	202	13.9	5.39	1.48	x
3	202	17.9	4.75	1.15	x
4–6	238	9.9	6.94	2.46	x
7–8	238	13.9	5.86	1.75	x
9–10	238	17.9	5.14	1.35	x
11–13	272	9.9	7.41	2.8	x
14–17	272	13.9	6.26	2.0	x
18–25	272	17.9	5.51	1.55	x
26	307	9.9	7.87	3.16	
27	307	13.9	6.65	2.25	
28–29	307	17.9	5.86	1.75	
30	346	13.9	7.06	2.54	

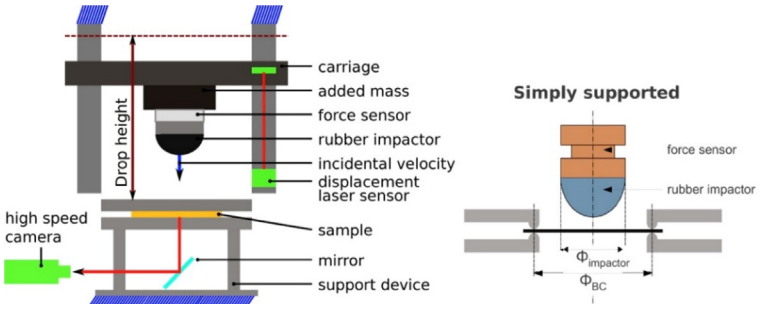

(a) Home made drop test tower (b) Rubber impactor and interlock target

Fig. 5. Experimental set-up.

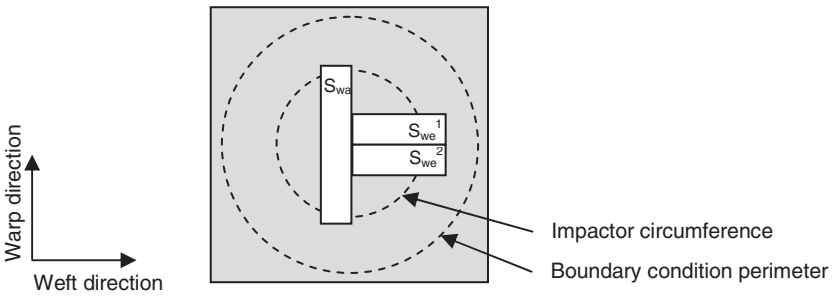

Fig. 6. Cut sections for microscopic observations.

ing damage in the warp direction whereas specimens noted S^1_{we} and S^2_{we} are used to observe damage in the weft direction.

5. Mechanical response of the plates subjected to soft impact loading

In the section, the mechanical response of the plates subjected to low velocity soft impact loading is studied. The responses of interest are the force–time, the displacement–time and the force–displacement relationships. Moreover, considerations on the impactor behavior during testing and the corresponding contact area are also discussed.

5.1. General comments

Typical force–time and force–displacement curves are shown in Figs. 7 and 8. In Fig. 7, the curves correspond to a case for which the plate underwent low level of damage. They are generally free of the usual oscillations which can be observed when testing with a rigid impactor at the beginning of the impact. The force–time curve (Fig. 7a) looks like a rather smooth bell shape. Small oscillations can appear when slight damages occur in the specimens. The force–displacement curve (Fig. 7b) can be divided into three parts. The first part, until point A, represents the evolution of the elastic

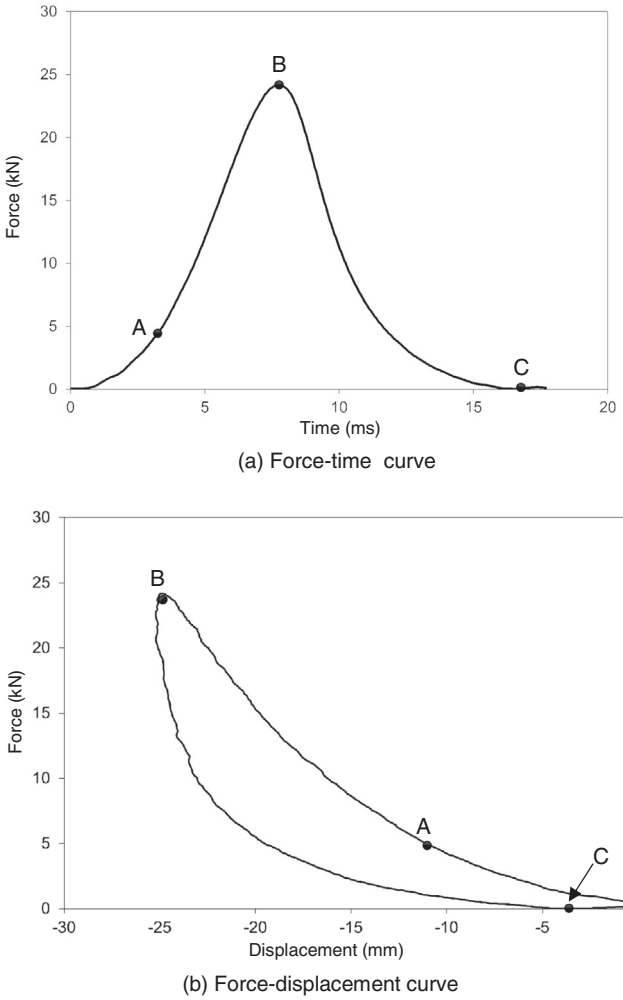

Fig. 7. Typical response of a composite plate tested at 202 J (M = 17.9 kg, test 3).

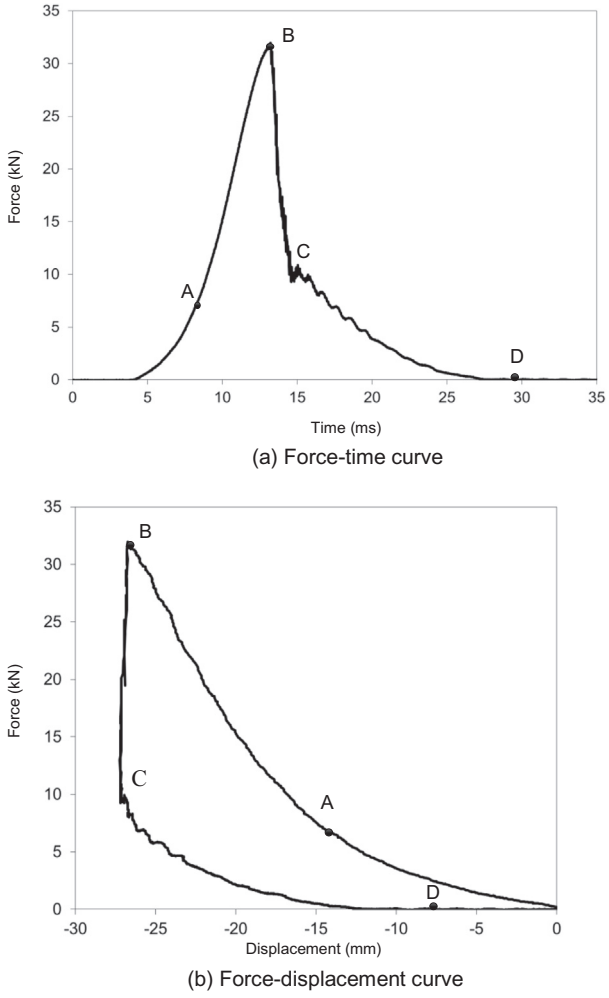

Fig. 8. Typical response of a composite plate that has perforated during testing at 272 J (M = 17.9 kg, test 20).

rigidity of the system. The non-linear evolution is a characteristic of both the non-linear elastic material and geometrical behavior of the rubber impactor during impact. The second part of the curve, between points A and B, corresponds to the deflection of the plate under impact. As damage develops in the plate, some small oscillations in the measured force can be observed. The amplitude of these oscillations depends on the nature and the amplitude of induced damage. This part will be addressed in the impact damage section. The maximum force is reached at point B which corresponds to the maximum carriage displacement. Then the force and displacement start decreasing as the impactor rebounds and contact between the plate and the impactor is lost. This corresponds to the last part of the curve between points B and C.

Fig. 8 represents typical force–time and force–displacement curves for a plate that perforated during impact. In that case, four separate parts can be pointed out. The first parts of the curves until point B, are similar to the ones shown in Fig. 7. However, as the maximum force is reached at point B, a sudden drop in the force occurs until point C. This corresponds to a sudden loss of strength induced by perforation of the plate as indicated by the video observation. When perforation occurs, the carriage displacement continues increasing slightly until point C at which perforation process stops. Then, depending on the test, the force and the displacement can either slightly increase again before definitively decreasing or directly decrease until contact loss between the plate and the impactor. This is the last part of the curves between points C and D. As expected, the contact time is longer when perforation occurs.

An example of the deformation of the rubber impactor captured by a high speed camera during impact is shown in Fig. 9. As observed in the figure, the elastic deformation is significant which means that the amount of elastic energy stored in the impactor is high.

Besides, the significant elastic deformation of the impactor induces a significant contact area between the impactor and the plate. For all tests, the maximum contact area is assessed by the blue chalk print made by the impactor on the paper taped on the plate, as shown in Fig. 9. The shapes of these prints are quite circular and can be characterized by their diameter, Φ_{contact}. Overall, the measured diameters ranged from 74 mm to 80 mm. The smallest ones corresponds to the tests conducted at 202 J incident energy. For the tests conducted at higher incident energies, all diameters were closed and ranged from 78 to 80 mm with no clear relationship between the incident velocity and mass of the impactor. By comparing the unit cell dimensions of the interlock material with the contact area diameter, it is found that in the warp direction the ratio range is

$$1.48 \leqslant \frac{\Phi_{contact}}{L_{warp}} \leqslant 1.60$$

and in the weft direction the ratio range is

$$7.4 \leqslant \frac{\Phi_{contact}}{L_{weft}} \leqslant 8.0.$$

As a consequence, variability is expected to be observed in the results as the ratio is small especially in the warp direction.

5.2. Repeatability study of the impact response

5.2.1. Justification

The repeatability study was conducted at a 272 J incident energy using a mass impactor of 17.9 kg. That level of energy was selected because previous tests (tests 18 to 21 in Table 1) showed some discrepancies in the damage tolerance of the composite material. A more thorough study was needed to investigate this issue. Four additional tests (tests 22 to 25 in Table 1) were carried out. The four specimens were cut from the same composite plate and tested under the same impact test conditions one after the other. It was unfortunately not possible to perform more tests due to a lack of availability of the composite material.

5.2.2. Results

The force–time curves obtained for the four tests are presented in Fig. 10. The curves for tests 22 and 23 have a rather smooth bell shape which seems to indicate that a low level of damage occurred. The first part of the curves for tests 24 and 25 are smooth but after the peak oscillations reveal that severe damage has occurred. Note that the slopes of the curves are identical before the peak for tests 22, 23 and 25. The different slope observed for test 24 is probably due to an erroneous experimentation. Pictures of the backside of the plates are shown in the figure. The plate of test 22 has no external visible damage whereas the plate of test 23 is clearly damaged on the backside. However, the force–time curves are identical for the two plates. Plates of tests 24 and 25 have been so severely damaged that they have perforated.

The carriage displacement as a function of time obtained for the four tests is presented in Fig. 11. The displacement decreases with time and reaches zero as the impactor hits the specimen (point A). It is interesting to note that the slopes are identical for tests 22, 23, and 25. This means that the impactor hits the specimen at the same speed estimated equal to 5.5 m/s from the experimental data. This value is the same as the theoretical one. However, for test 24, the slope is much lower and corresponds to a speed equal to 3.98 m/s at point A. Reason for this deviation is probably due to an erroneous experimentation as mentioned above. It explains that the force–time curve for test 24 does not follow the same trend as for the other tests. Looking at the carriage displacement curve for the three other tests, one can note that the carriage rebounds from the specimen at different speeds. The more the plate is damaged, the lower the speed of the carriage is and the longer the contact time between the impactor and the plate is. In addition, note that the maximum carriage displacement is nearly the same for every test.

Fig. 12 shows the contact force as a function of carriage displacement for the four repeated tests. Interesting results are observed. Up to the maximum force, the curves are perfectly superposed which indicates that the elastic stiffness of the system

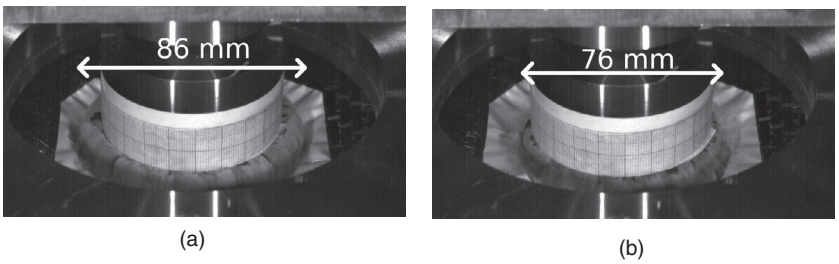

Fig. 9. Example of the rubber impactor deformation (ΔT = 0.7 ms between the two images): (a) at the maximum force just before perforation; (b) just after plate perforation.

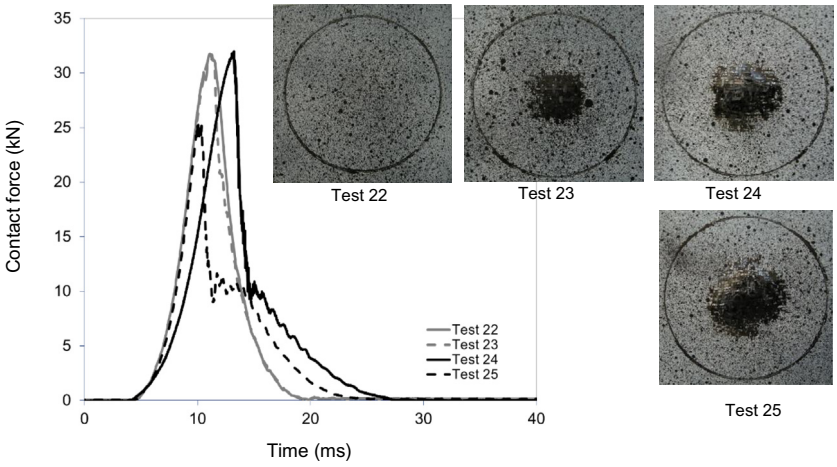

Fig. 10. Contact force versus time at 272 J (Interlock 3X 55% woven composite).

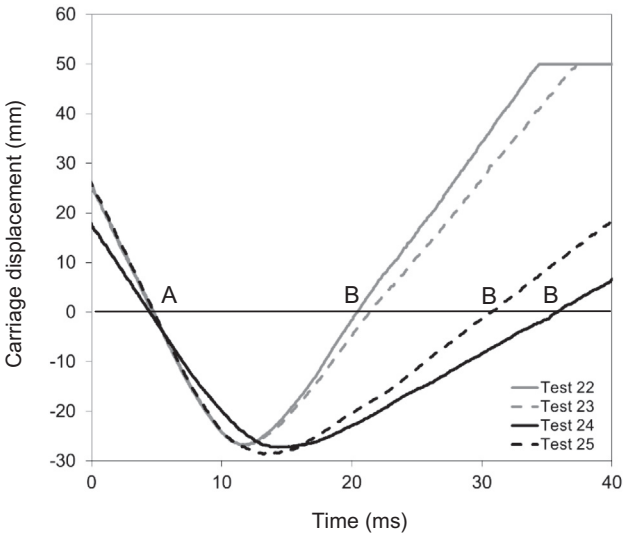

Fig. 11. Carriage displacement versus time at 272 J (Interlock 3X 55% woven composite).

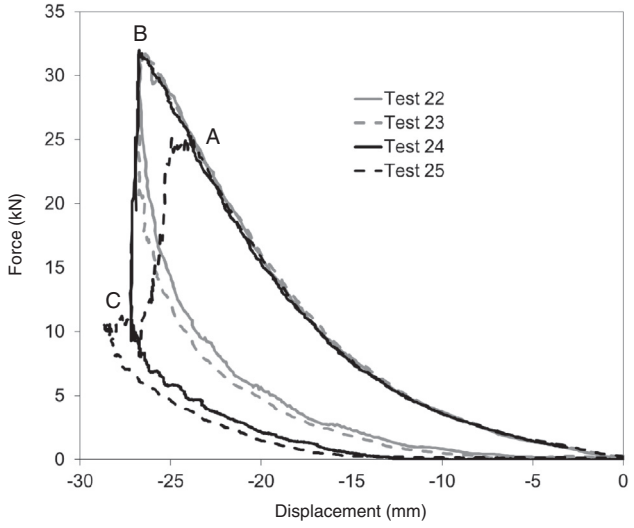

Fig. 12. Force-carriage displacement curve at 272 J (Interlock 3X 55% woven composite).

is actually identical for the four tests. The maximum force reached for test 25 is the lowest (point A). For the three other tests, the maximum force is similar (point B). Then, for tests 22 and 23, the force and the displacement decrease quite smoothly in a similar fashion. These curves correspond to the two plates that have a low to moderate damage level. For test 24, the force drops abruptly and reaches the force–displacement curve of test 25 (point C). Then, the force and the displacement decrease in a similar fashion. Therefore, the results of test 25 which appeared to be erroneous when represented as a function of time in Figs. 10 and 11 are in fact consistent with the results obtained for the three other tests.

5.2.3. Concluding remarks

This study showed that damage extend due to impact can vary even though the test conditions are identical. Reasons for this deviation can come from different sources. First, it has been established by previous measurement tests that the carriage velocity can undergo variation up to 5% which means that a nominal velocity of 5.5 m/s can range from 5.22 m/s to 5.77 m/s. This translates into an incident energy that may range from 244 J to 298 J. Next, the rubber impactor may not have exactly the same mechanical behavior from one test to the other. Finally, as observed in Section 2.2, the interlock 3X woven composite is a material which is heterogeneous on a large scale. The matrix is not evenly distributed which leads to resin-rich areas. The textile pattern is not perfectly repeated and uniform due to the RTM process. The inclusion of interlacing yarns in a 3D woven composite also affects significantly the internal structure. All these factors influence greatly the mechanical properties and residual strengths of the composite. Some studies [19–22] underlined the yarn waviness as a key role in the strength reduction in the 3D woven composites.

Moreover, the representative unit cell (50 mm × 10 mm) is very large compared to the impactor size (70 mm in diameter). The position of the unit cells on the contact zone under the impactor may be an important factor that can influence the response of the specimen.

5.3. Velocity effect at constant mass (13.9 kg) on the impact response

5.3.1. Selected tests

Results of the tests performed with a constant mass of 13.9 kg were used to study the effect of the impactor velocity on the plate response. The choice of this mass was arbitrary. The impactor velocity was varied from 5.39 m/s to 7.06 m/s to obtain five incident energies (202 J, 238 J, 272 J, 307 J and 346 J). The tests used for this study correspond to tests 2, 7, 17, 27 and 30 in Table 1.

5.3.2. Results

The force–time curves are plotted in Fig. 13. As the incident energy increases which translates into a velocity increase, the maximum contact force gets higher and higher until a critical value is reached. The damage level induced in the plate becomes more important as the maximum load increases. For an energy level higher than 272 J, the plate is so damaged that it perforates. The critical energy for perforation ranges between 272 J and 307 J.

Besides, the contact duration for the various incident energies are very close as long as the plate doesn't perforate. This behavior is different from what is usually observed when using a rigid impactor. In that case, the contact decreases as the incident velocity increases. The difference in the behavior is explained by the high capacity of absorption of the rubber impactor.

Fig. 14 represents the carriage displacement as a function of time for the five energy levels. The carriage displacement reaches zero as the impactor hits the specimen. Since the velocity increases with the incident energy, the initial slope of the curves increases as can be observed in the figure. Moreover, the maximum displacement increases with the incident energy until a critical value is reached. This correlates well with the contact force increase observed in Fig. 13. After the maximum displacement is reached, the carriage rebounds at different speeds. The rebound speed increases with the incident energy as long as it is not larger than 272 J. For larger values, damage induced in the specimen is more significant and the rebound speed is much lower.

Fig. 15 shows the contact force as a function of carriage displacement for the five energy levels. The specimen impacted with the smallest incident energy responds more quickly as evidenced by the contact force that starts increasing at lower carriage displacement. This is probably due to the rubber impactor that deforms less at a lower impact energy. As the impact energy increases, the peak load, the maximum displacement and the absorbed energy increase. When the impact energy is higher than 272 J, the displacement keeps increasing slightly after the peak load which is due to the plate perforation. After the perforation process ends, the displacement decreases until the force reaches zero.

5.3.3. Concluding remarks

As the incident velocity increases for a constant impactor mass, the impact energy increases which induces an increase of the peak load and the maximum carriage displacement. The energy absorbed (area within a curve) by the impactor/specimen system is higher which is due to the development of internal damages in the specimen. As a critical value is reached, the specimen is so damaged that it perforates.

5.4. Mass–velocity effect at constant energy on the impact response

5.4.1. Selected tests

The objective of this study is to investigate the effect of the mass/velocity couple on the impact response of the specimens. Tests were performed with three incident energies: 202 J, 238 J and 272 J. The incident energy of the impactor was imposed by selecting the appropriate impactor mass/incident velocity couple. For each energy level, three different mass/incident velocity couples were used. Referring to Table 1, the tests for the 202 J incident energy correspond to tests 1, 2 and 3. The tests for the incident energy of 238 J are numbered 4, 7 and 9. Finally, the tests for the 272 J incident energy correspond to 12, 14 and 19 in the table.

The contact force and the carriage displacement measured during impact will be analyzed and micrographs of cross-sections of

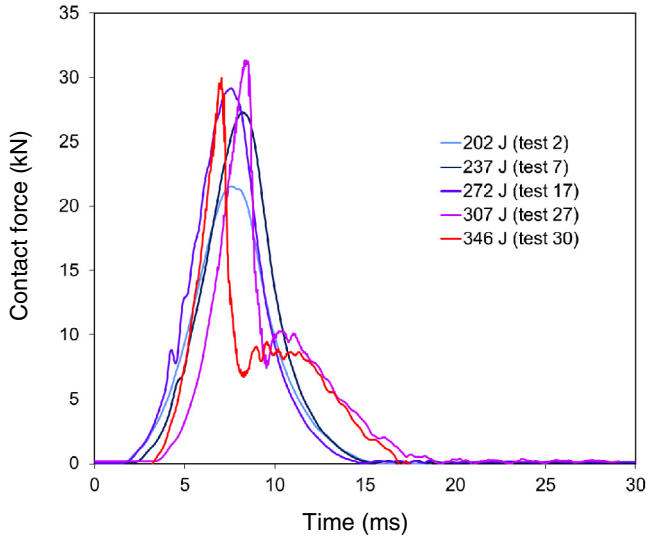

Fig. 13. Contact force versus time for $M = 13.9$ kg.

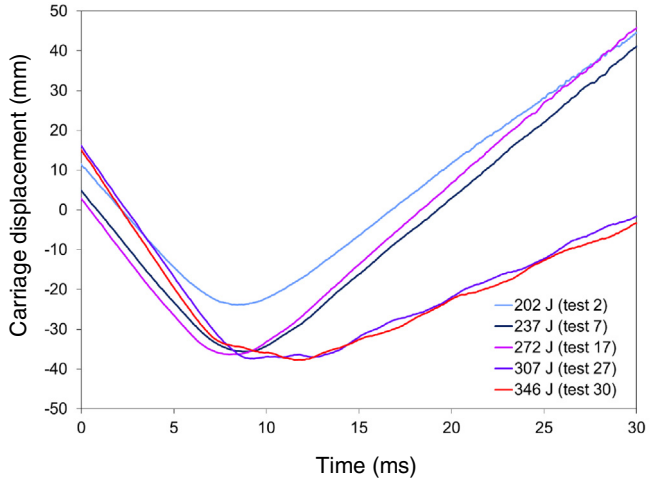

Fig. 14. Carriage displacement versus time for $M = 13.9$ kg.

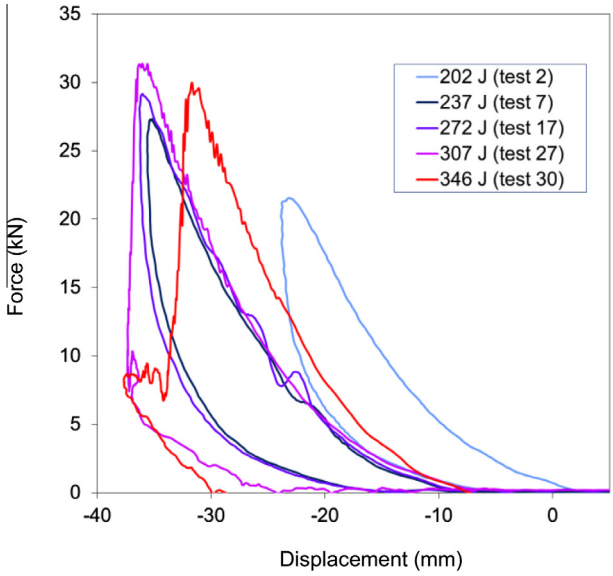

Fig. 15. Force-carriage displacement curve for $M = 13.9$ kg.

impacted specimens will be observed to assess the effect of the mass/velocity couple. However, the micrographs will be presented in the next section dedicated to damage analysis.

5.4.2. Results

The force–time curves and the carriage displacement–time curves obtained for the three energy level are presented in Figs. 16–18. The force–time curves have a rather smooth bell shape which indicates that not too much severe damage has occurred. As the mass is increased, the contact force increases from 21 to 24 kN and from 27 to 33 kN for the tests at 202 J and 272 J, respectively. For the 238 J tests, the force increases from 27 to 29 kN as the mass increases from 9.9 to 13.9 kg but then decreases slightly for a 17.9 kg mass. For that mass, a small oscillation can be observed on the curve which may be due to occurrence of damage in the specimen. Moreover, the force–time curves show that the force increases more rapidly when the mass is low and that the contact between the impactor and the plate lasts longer when the mass is increased. These observations are expected since the impactor speed decreases with increasing mass.

Looking at the force–displacement curves, it appears that the stiffness of the impactor/specimen system is not the same when the mass is increased. However, the amount of energy absorbed by the system is quite similar. These results show that the system response is somewhat modified when different mass/velocity couples are used to generate the same energy level. The microscopic observations of the impacted specimen cross-sections will allow to assess if these changes translate into differences in the type of damage induced in the specimens.

6. Damage analysis

6.1. Damage observations and rupture scenario

Micrographs of the cross-section of the specimen impacted at a 272 J incident energy ($M = 17.9$ kg) are shown in Fig. 19. The damages that can be observed are intra-yarn cracks, matrix cracks, yarn debonding and yarn ruptures. Matrix cracks refer to the cracks which appear in the inter-yarn zones filled with resin only. These different damage modes interact with each other. As can be

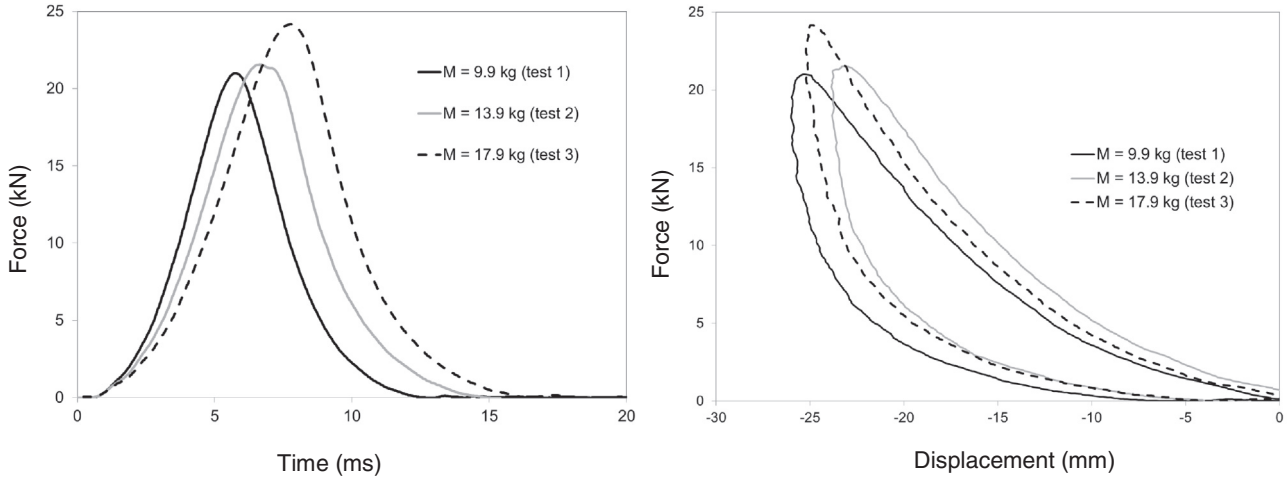

(a) Force-time curves (b) Force-displacement curves

Fig. 16. Effect of the mass/velocity couple for a 202 J incident energy tests.

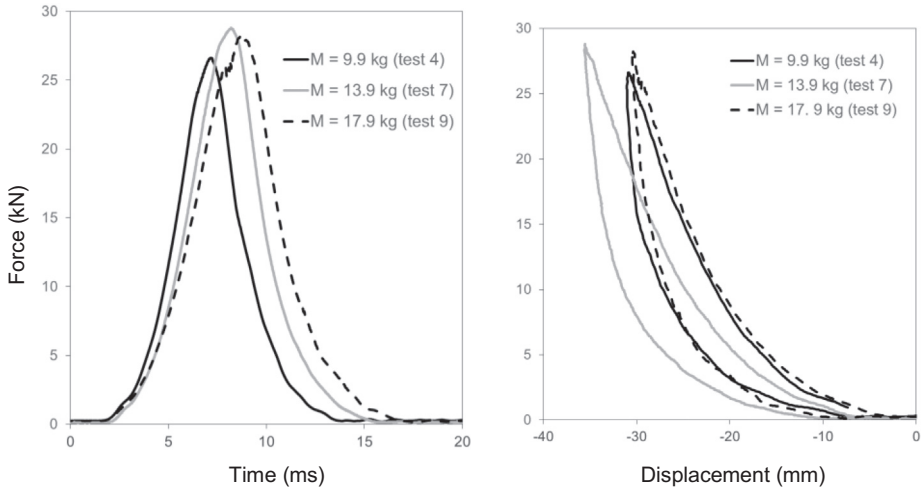

(a) Force-time curves (b) Force-displacement curves

Fig. 17. Effect of the mass/velocity couple for a 238 J incident energy tests.

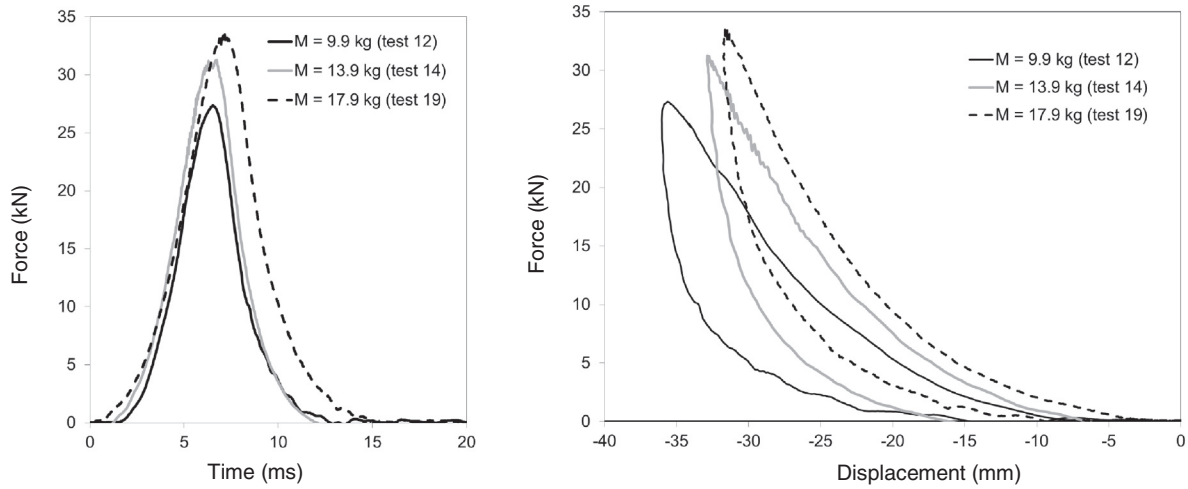

(a) Force-time curves (b) Force-displacement curves

Fig. 18. Effect of the mass/velocity couple for a 272 J incident energy tests.

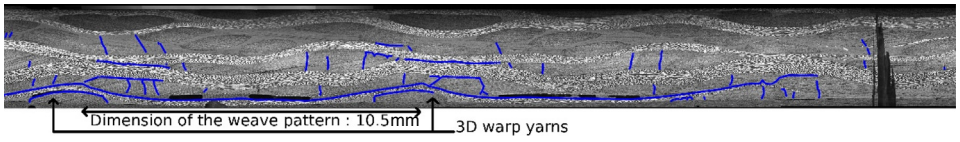

(a) Along the weft direction

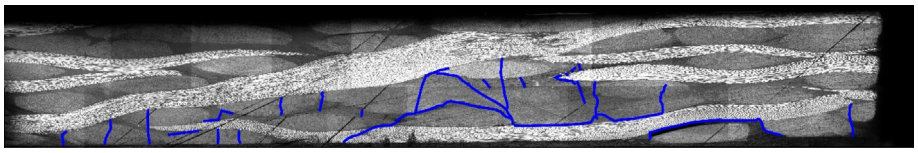

(b) Along the warp direction

Fig. 19. Micrographs of the cross-section of an impacted specimen (272 J, test 19).

observed on both micrographs, damage mostly develops in the lower half of the specimen cross-section at the opposite of the impacted side. The damaged area is important and represents around 1/2 to 3/4 of the contact area (impactor/plate). Damages do not form a conical shape as it is usually the case for specimens tested with rigid impactors [23,24]. It can be explained by the fact that, with a deformable impactor, the contact area is much larger which induces much less stress concentration in the material under the contact area during testing. Under this area, the sample is a priori mainly loaded in bending. However, numerical simulations are necessary to validate this assumption. Therefore, the lower half of the specimen is mostly subjected to tensile stresses whereas the upper half is mostly under compressive stresses. Damages are mainly observed in the lower half of the specimen which means that they are induced by tensile stresses.

Looking at Fig. 19(a) which represents the cross-section along the weft direction, long decohesions are visible at the interface of the weft yarns closest to the bottom side of the specimen. Cracks can be observed in the lower half as well as in the upper half of the specimen.

As shown in Fig. 19(b), the cross-section along the warp direction show several adjacent weft yarns surrounded by straight and 3D warp yarns. Multiples cracks are observed in these regions, mainly on the lower half of the specimen. However, these cracks have also spread from the bottom toward the upper half of the specimen in the absence of warp yarns to stop their progression. The intricacy of the crack pattern is a sign of the complexity of the stress field induced by the warp yarns, especially the 3D warp yarns.

Fig. 20 presents the force measured as a function of time for a 307 J impact test as well as photos of the back of the specimen taken with the high speed camera (see Section 3) during impact. A scenario for the rupture process can be supposed from the results presented in this figure.

As can be observed in the figure, the peak load is reached at time $t = 5$ ms. The photo taken at that time shows that no significant damage is visible on the back side of the specimen. Between $t = 5$ ms and $t = 5.1$ ms, the load starts decreasing and damage becomes visible on the backside of the specimen. The rupture process has begun. On the photo, yarn decohesions are clearly visible. The perforation process seems to initiate with the rupture of the 3D warp yarns.

6.2. Mass–velocity effect at constant energy on damage state

The damage state induced in specimens impacted at a constant energy but using different mass/velocity couples is investigated. For the sake of brevity, only the results for the 202 J energy level will be presented.

Fig. 21 presents microscopic observations of damages that occurred along the weft direction. The impactor radius (R) is indicated. Different damage modes can be seen, in particular transverse cracks in the matrix and in the yarns, longitudinal cracks in

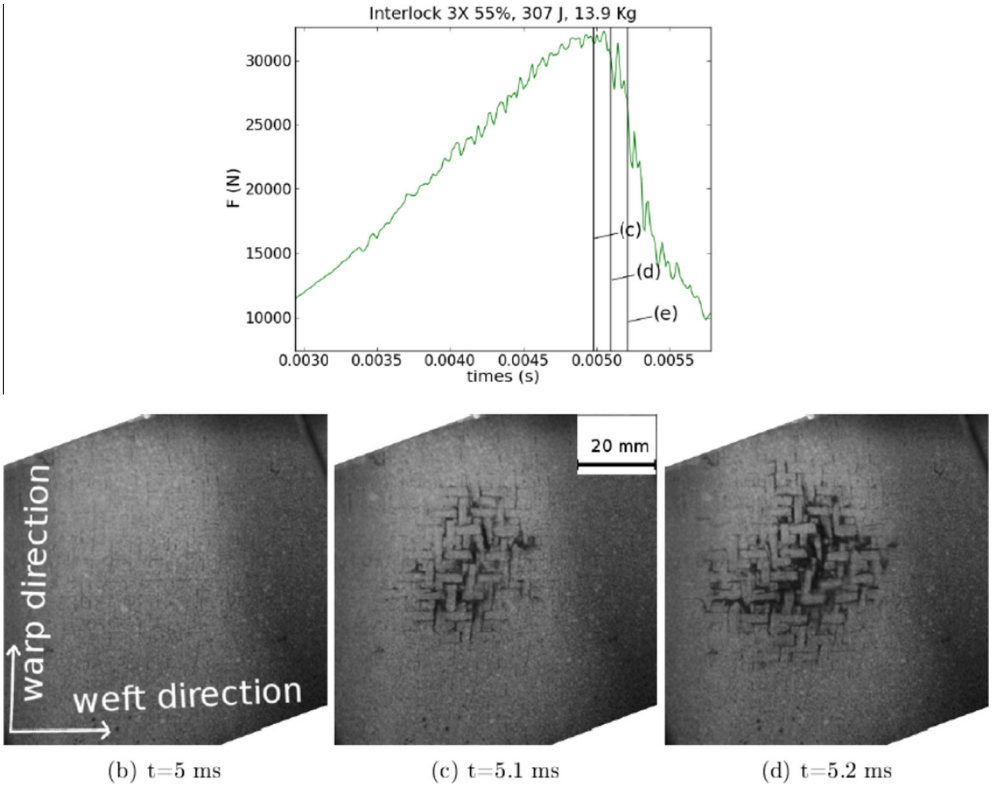

Fig. 20. Evolution of the plate response and the perforation process (307 J, test 27).

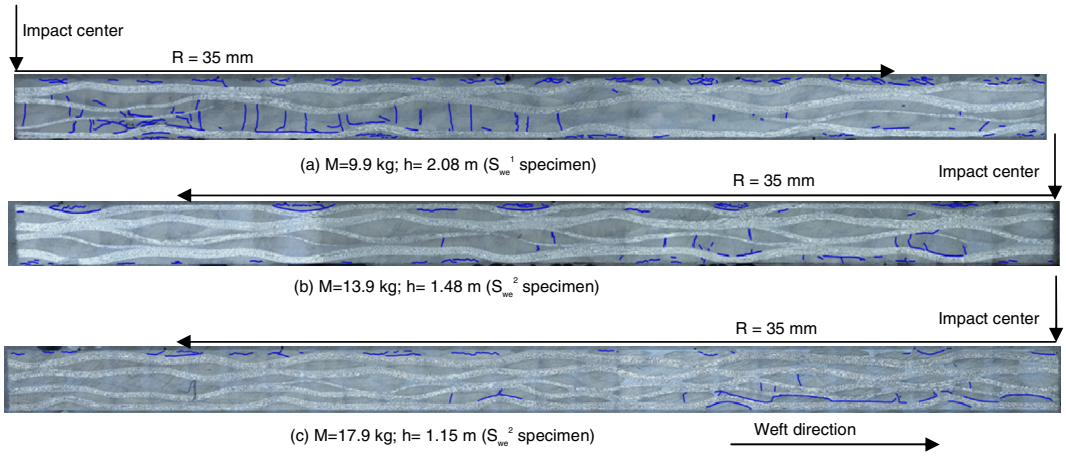

Fig. 21. Damages observed along the weft direction (202 J).

the upper warp yarns, and matrix-yarns debonding. As the mass increases, fewer cracks in the matrix and yarns are present and more yarn debonding is observed near the surface opposed to the impacted one. The warp yarns (whose cross-sections are visible in the picture) located near the impacted surface are less damaged as the mass increases.

Fig. 22 presents microscopic observations of damages that occurred along the warp direction. The impactor diameter (Φ) is indicated. Transverse matrix and yarn cracks are present for the three cases. As the mass increases, fewer longitudinal cracks in the upper weft yarns are present. Warp yarn decohesions are visible for the three mass/velocity couples but the location changes. For $M = 9.9$ kg, yarn decohesion are localized under the impact close to the lower surface. As mass increases, yarn decohesions are still close to the lower surface but are spread over a wider zone away from the impact center.

For this energy level, as observed in Fig. 16, the force–time curves have a rather smooth bell shape. Therefore, damages observed on the micrographs are not revealed by the specimen macroscopic response. Nevertheless, they can have non negligible effects on the composite residual strength.

Damage state observed on the micrographs for the two other levels of impact energies (237 J and 272 J) is not fundamentally different from damage induced by a 202 J incident energy. The additional energy doesn't seem to necessarily generate more damage but rather result in larger impactor deformation and higher contact force. However, specimens impacted with an incident energy higher than 272 J are definitely more damaged and have

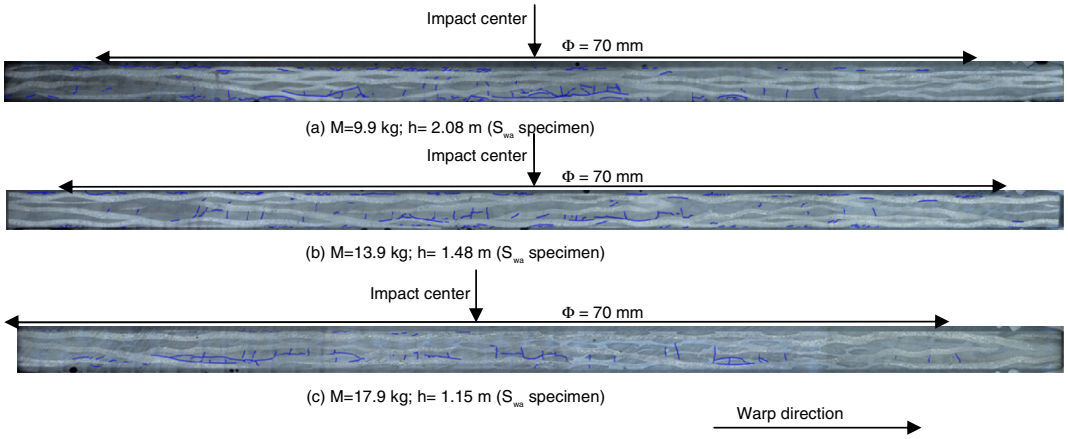

Fig. 22. Damages observed along the warp direction (202 J).

all perforated (tests 26 to 30 in Table 1). In these cases, the impactor which is completely crushed behaves like a rigid impactor and the additional energy is absorbed by the creation of severe damages in the matrix and in the yarns.

7. Conclusions

This study investigated the mechanical behavior and damage characteristics of a three-dimensional (3-D) woven composite subjected to a low velocity impact by a highly deformable rubber impactor.

Several impact tests were performed at energy levels varying from 202 J to 346 J obtained with different mass/incident velocity couples. The experimental results, based on load-time, displacement–time and load–displacement curves, allowed to identify a critical threshold energy for the composite material perforation.

Variability issues due to different sources were highlighted. Variations up to 5% on the velocity measurements, the evolution of the rubber impactor behavior, the lack of uniformity and repeatability of the textile representative unit cell due to the RTM process but also the location of impact on the representative unit cell can influence greatly the performance of the 3-D woven composite under soft impact loading.

Besides, the analysis of the force–time and the carriage displacement–time curves and the mass-velocity effect study confirmed expected tendencies. It could be noticed that even though the force–time curve has a rather smooth bell shape, quite significant damage can occur. Finally, microscopic observations of damages along both the weft and warp directions showed transverse cracks in the matrix and in the yarns, longitudinal cracks in the upper warp yarns, and matrix-yarns debonding. They also revealed that the damage mechanisms were influenced by the mass/velocity couples. Parallel to this present work, numerical investigations have been carried out and will be presented in a forthcoming paper.

References

[1] Abrate S. Impact on composite structures. Cambridge University Press; 2005.
[2] Cantwell W, Morton J. The impact resistance of composite materials – a review. Composites 1991;22(5):347–62.
[3] Richardson MOW, Wisheart MJ. Review of low velocity impact properties of composite materials. Compos A Appl Sci Manuf 1996;27(12):1123–31.
[4] Davies GAO, Olsson R. Impact on composite structures. Aeronaut J 2004;108 (1089):541–63.
[5] Potluri P, Hogg P, Arshad M, Jetavat D, Jamshidi P. Influence of fiber architecture on impact damage tolerance in 3D woven composites. Appl Compos Mater 2012;19(5):799–812.
[6] Zhijiang L, Baozhong S, Bohong G. FEM simulation of 3D angle interlock woven composite under ballistic impact from unit cell approach. Comput Mater Sci 2010;49(1):171–83.
[7] Lv L, Sun B, Qiu Y, Gu B. Energy absorptions and failure modes of 3d orthogonal hybrid woven composites truck by flat-ended rod. Polym Compos 2006;27 (4):410–6.
[8] Byun JH, Song SW, Lee CH, Um MK, Hwang BS. Impact properties of laminated composites with stitching fibers. Compos Struct 2006;76(1–2):21–7.
[9] Luo Y, Lv L, Sun B, Qiu Y, Gu B. Transverse impact behaviour and energy absorption of three-dimensional orthogonal hybrid woven composites. Compos Struct 2007;81(2):202–9.
[10] Ji C, Sun B, Qiu Y, Gu B. Impact damage of 3d orthogonal woven composite circular plates. Appl Compos Mater 2007;14(5):343–62.
[11] Johnson AF, Holzapfel M. Modelling soft body impact on composite structures. Compos Struct 2003;61(1–2):103–13.
[12] Lavoie MA, Gakwaya A, Nejad Ensan M, Zimcik DG, Nandlall D. Bird's substitute tests results and evaluation of available numerical methods. Int J Impact Eng 2009;36(10–11):1276–87.
[13] Dau F, Duplessis Kergomard Y. Damage mechanisms in interlock 3X woven composites under low velocity soft impact loading. In: Composite materials and structures: the way forward, proceeding of the 26th ASC technical conference/2nd joint US-Canada conference on composites, Montreal, 26–28 September 2011.
[14] Heimbs S, Van Der Broucke B, Duplessis Kergomard Y, Dau F. Rubber impact on 3D textile composites. Appl Compos Mater 2012;19(3):275–95.
[15] Duplessis-Kergomard Y, Dau F, Heims S. Choc mou basse énergie sur composite interlock 3X: approche expérimentale et numérique. Rev Matér Techniq 2012;100(6–7):6–7.
[16] Bassi AC, Casa F, Menditchi R. Shore A hardness and thickness. Polym Testing 1987;7(3):165–75.
[17] Harwood JAC, Mullins L, Payne AR. Stress softening in rubbers: review. Inst Rubber Indus J 1967;1(1):17–9.
[18] Boussu F, Cristian I, Nauman S. General definition of 3D warp interlock fabric architecture. Compos B 2015;81:171–88.
[19] Chou S, Chen HC, Chen HE. Effect of weave structure on mechanical fracture behaviour of three-dimensional carbon fiber fabric reinforced epoxy resin composites. Compos Sci Technol 1992;45(1):23–35.
[20] Leong KH, Lee B, Herszberg I, Bannister MK. The effect of binder path on the tensile properties and failure of multilayer woven CFRP composites. Compos Sci Technol 2000;60(1):149–56.
[21] Kuo WS, Ko TH, Chen CP. Effect of weaving processes on compressive behaviour of 3D woven composites. Compos A Appl Sci Manuf 2007;38 (2):555–65.
[22] Mcllhagger R, Quinn JP, Mcllhagger AT, Wilson S, Simpson D, Wenger W. The influence of binder tow density on the mechanical properties of spatially reinforced composites. Part2: mechanical properties. Composite Part A 2008;39(2):334–41.
[23] Shyr TW, Pan YH. Impact resistance and damage characteristics of composite laminates. Compos Struct 2003;62(2):193–203.
[24] Mitrevski T, Marshall IH, Thomson R. The influence of impactor shape on the damage to composite laminates. Compos Struct 2006;76(1–2):116–22.